Systematic analysis of above-barrier fusion of ^{9,10,11}Be + ^{209}Bi

D. J. Hinde and M. Dasgupta

Department of Nuclear Physics, Research School of Physics and Engineering, Australian National University,
Canberra, ACT 0200, Australia

Measurements of fusion for ^{9,10,11}Be allow testing of the relative importance to fusion and breakup of the α-cluster structure found in all these Be isotopes, compared with the neutron-halo structure only present for ^{11}Be. However, disagreements exist among different published experimental data sets for the reactions of ^{9,10,11}Be with ^{209}Bi. Accurate measurements of above-barrier cross sections for the products of complete fusion (fission and evaporation residues) in the reaction of ^{9}Be with ^{209}Bi and ^{208}Pb provide the basis for a reanalysis of above-barrier fusion for ^{10,11}Be + ^{209}Bi. This includes procedures making full use of the higher precision stable beam data and resolves many of the disagreements. The improved self-consistency of the analysis allows investigation of the experimental average fusion barriers. Although showing some scatter, these suggest a higher barrier for the neutron halo nucleus ^{11}Be. Comparison of published cross sections for fusion associated with capture of all the charge of the projectile suggest that all these Be isotopes show significant suppression of complete fusion, a surprising result given that the α-breakup threshold energies are 1.57 MeV for ^{9}Be but over 7 MeV for ^{10,11}Be. Further experimental studies to investigate in more detail the division between complete and incomplete fusion for reactions of ^{10,11}Be are needed.

I. INTRODUCTION

The reaction dynamics of weakly bound nuclei has received renewed attention in recent years [1], with the increasing availability of beams of weakly bound radioactive nuclei with exotic matter distributions, particularly neutron halos. Light nuclei near the valley of stability can also show "exotic" matter distributions, owing to the strong binding of the α particle. The clearest example is ^{8}Be, comprising two α particles, unbound by 92 keV. Both experiments and theoretical calculations [2] show that the heavier (bound) Be isotopes also have a strong α-cluster structure, including the halo nucleus ^{11}Be.

The study of near-barrier complete and incomplete (partial) fusion gives insights into the dynamical behavior of these nuclei in the last stages of the collision, just before capture by the (generally heavier) target nucleus. Fusion of ^{11}Be should be a particularly interesting case, as it should reveal the relative importance of the neutron halo and α-cluster structure on the fusion dynamics.

Studies of the lighter ^{9}Be have provided many definitive insights into reaction dynamics. Measurements of complete fusion [3,4] for the reaction ^{9}Be + ^{208}Pb gave the first direct evidence of suppression of complete fusion. A critical step in reaching this conclusion was to determine experimentally the average fusion barrier energy (or barrier distribution centroid) and to ensure that all calculations reproduced this value. Without this constraint, enhancement or suppression of the measured complete fusion cross sections with respect to the calculations can be obtained according to the choice of the (unconstrained) nuclear potential and/or couplings [5]. Complete fusion (CF) with ^{9}Be (and ^{6,7}Li) projectiles has been generally defined experimentally as absorption of all the charge of the projectile, since it is difficult to measure whether a neutron was not captured without actually detecting it in coincidence with the heavy fusion product. Furthermore,

without a repulsive Coulomb field between a weakly bound neutron and the heavy target nucleus, at near-barrier energies we might expect the neutron to fuse with high probability. This definition of complete fusion, also used in this work, allows separation if incomplete fusion (ICF) and complete fusion (in reactions with heavy nuclei such as ^{209}Bi) on the basis of the atomic number of the heavy product [3,4,6]. The capture of a single $Z = 2$ fragment, independent of its mass, will be referred to in this work as α-ICF. The studies mentioned here, and others, concluded that at above-barrier energies CF cross sections are suppressed by $\sim$30%, compared with the predictions of both the single barrier penetration model (SBPM) and the coupled-channels (CC) model, under the assumption of no breakup [3–10].

Supporting evidence of the suppression of complete fusion came from the large yields of heavy products, intermediate in mass between that of the target and the products of complete fusion. They were consistent with the products expected following incomplete fusion [3,6]. However, from these measurements alone, it could not be excluded that the heavy products assigned to incomplete fusion might have been produced directly by transfer reactions. This was addressed [11] by making measurements of α particles resulting from reactions of ^{9}Be with Pb and Au targets at subbarrier energies. Here the cross sections of heavy products of α-incomplete fusion had been measured [3] to be negligible. Nevertheless, large cross sections for α-particle production were observed. A significant part of this yield was unambiguously assigned to delayed (sequential) breakup of ^{8}Be nuclei from the ground state. Their long lifetime ($\sim$10^{-16} s) means that their breakup cannot affect fusion. The remaining yield was associated with prompt breakup [11] of the projectile close to the target, resulting for example from breakup of excited states or direct coupling to the continuum. At above-barrier energies

this would reduce complete fusion and result in incomplete fusion; a qualitative assessment of the measured subbarrier breakup probabilities indicated they were sufficient to explain the above-barrier ICF [11]. Development of a classical two-dimensional three-body trajectory model [12] was followed by a three-dimensional model with stochastic breakup [13], which confirmed quantitatively that the below-barrier breakup probabilities are consistent with the above-barrier suppression of complete fusion.

Recent work [14] has shown that for ^{9}Be incident on a wide range of heavy target nuclei, prompt breakup is predominantly triggered by neutron transfer. Thus it is not only the properties of the projectile itself that are important, but also the probable transfer channels, and the properties of the nuclei and the states that are populated following transfer. This insight makes the prediction of breakup for any given projectile much more complex. This could change the expectations of the probability of ICF for the heavier Be isotopes and opens up questions of the relative importance or indeed the linking of the roles of the α-cluster structure and the neutron halo structure in the reaction dynamics of ^{11}Be. For ^{10}Be, although it is strongly bound, suggesting negligible suppression of complete fusion, expectations may also change. Following a neutron stripping reaction, the weakly bound nucleus ^{9}Be is formed. When populated in an excited state, it will undergo prompt breakup, leading to ICF.

With this new realization, in this work we investigate the consistency and adequacy of existing data for complete fusion and the sum of CF and ICF (defined as total fusion) for the reaction of ^{9,10,11}Be with ^{209}Bi, to understand the nature of fusion in these reactions. In particular, existing experimental above-barrier fusion cross sections for the reactions of the radioactive nuclei ^{10,11}Be with ^{209}Bi are reanalyzed with the aim of (i) investigating the influence of the neutron halo of ^{11}Be on the average fusion barrier energy, (ii) ascertaining whether the α-ICF probabilities are consistent with empirical trends, and (iii) determining whether further fusion studies are required for reactions of these nuclei. In carrying out this detailed analysis, methods are presented that can be useful in future comparisons of fusion data from isotopic chains, including reactions with low-intensity radioactive beams.

II. COMPARISON OF EXPERIMENTS

There has been a long-standing discrepancy between the complete fusion cross sections for the reaction ^{9}Be + ^{209}Bi [15] and ^{9}Be + ^{208}Pb [3,4], with extracted CF cross sections for the former being $\sim$20% larger than the latter. This problem was recently addressed in Ref. [16], where it was concluded that normalization problems in the earlier ^{9}Be + ^{209}Bi measurements appear to be the only consistent explanation. *Relative* yields of the various reaction channels measured in *all* ^{9}Be + ^{209}Bi experiments appear to be very consistent, and thus they are used in the present work to address specific problems that become apparent in the systematic comparison of the ^{9,10,11}Be + ^{209}Bi measurements described in the following. Absolute cross section comparisons are then made with the most recent ^{9}Be + ^{209}Bi data [16].

A. The ^{9}Be + ^{209}Bi experiment

The new measurements of complete fusion for the ^{9}Be + ^{209}Bi reaction, carried out at the Australian National University (ANU), are already described in some detail in Ref. [16], so will not be described here. In that work, a comparison of the dominant complete fusion products (evaporation residues following neutron evaporation, denoted xn evaporation residues) from different measurements was made independently of the absolute normalization by evaluating the fraction of the total xn cross section in a given channel at each beam energy or corresponding excitation energy. This comparison is shown in Fig. 1. It should be noted that the data labeled $2n$ (corresponding to the 9.005-MeV α decay of ^{216}Fr) is likely to include a component of incomplete fusion from the 9.080-MeV ^{213}At decay. The analysis of the new ANU measurements, presented in Ref. [16], determined the ^{216}Fr yield to be substantially less than that previously assigned, as shown by the lower diamond-shaped point. An approximate $2n$ trend line has been assigned guided by that data point.

All data sets from different experiments at different laboratories agree well and allow well-defined empirical expectations for the division of probability among different evaporation channels as a function of excitation energy. The trend lines, shown by the curves, for the $3n$, $4n$, and $5n$ channels are important in the present analysis. They were obtained empirically from the dense experimental points, with the only constraint that the energy dependence should be smooth without local variations in curvature. They are used to give an empirical guide to expectations for the ^{10,11}Be + ^{209}Bi reactions in Sec. III, allowing reinterpretation of the experimental results for these reactions. Unlike statistical model calculations, these empirical curves will account for small effects of pre-equilibrium neutron emission [3], which should be present to a similar extent for each Be projectile, but
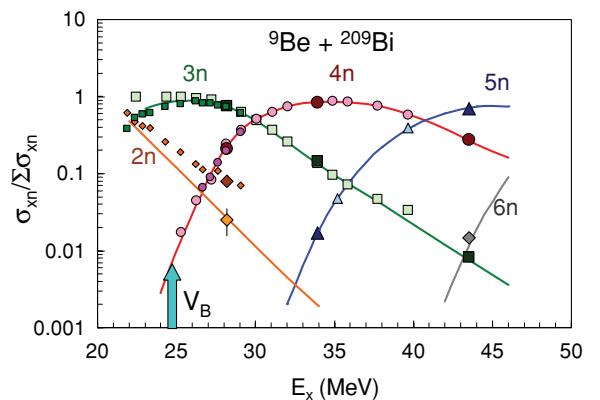

FIG. 1. (Color online) Experimental ratios of a given complete fusion xn evaporation product to the sum of all such products for the reaction ^{9}Be + ^{209}Bi, as a function of compound nucleus excitation energy E_x. The small symbols correspond to the data of Ref. [15], the intermediate symbols correspond to those of Ref. [17], and the largest symbols represent the recent measurements presented in Ref. [16]. All are in good agreement, showing that the disagreement among experiments can only be due to absolute normalization. The smooth curves describe the trends of these data and are used in the subsequent analysis (see text).
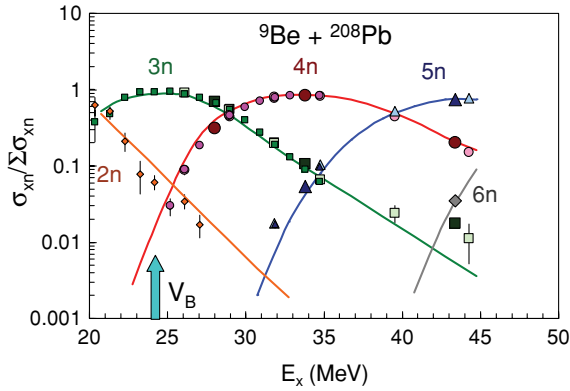
FIG. 2. (Color online) The same as Fig. 1, but for the reaction ^{9}Be + ^{208}Pb. The small symbols correspond to the data of Ref. [4], the intermediate symbols correspond to those of Ref. [3], and the largest symbols represent the recent measurements of Ref. [16]. The smooth curves are those from Fig. 1 (see text).

which could probably not be reliably calculated. The validity of applying these systematics to a different reaction can be tested using the extensive data [3,4,16] for the reaction ^{9}Be + ^{208}Pb. These are shown in Fig. 2, where the E_x values for the curves from Fig. 1 have been shifted according to the difference in the (fusion, 4n) Q value between the two reactions of 1.25 MeV (see also Sec. III). The curves describe the data for the different reaction extremely well, supporting their use for ^{10,11}Be.

B. The ^{10,11}Be + ^{209}Bi experiments

Experimental results for the reactions ^{10,11}Be + ^{209}Bi are presented in Refs. [17,18], from measurements carried out at RIKEN, Japan. Two separate experiments were carried out, described in Ref. [17] (published in 1996) and Ref. [18] (published in 2004). These will subsequently be denoted as Run 1 (R1) and Run 2 (R2), respectively. Beam energies around the barrier were obtained by degrading the initial ^{10,11}Be energies, resulting in a broad energy spread [18]. By measuring the flight time of each ^{10,11}Be beam particle prior to interacting with the target, the projectile energy was determined event by event. The identity and yields of the heavy fusion products were measured by counting the α particles emitted in their ground-state decays. The requirement to correlate the tagged beam particle with the subsequent α decay (to associate the decay with a specific beam energy) meant that only decays occurring within a certain time window after fusion could be used. This time window in turn determined the efficiency with which the various fusion-evaporation channels could be measured in these experiments.

Substantial differences between the reported experimental cross sections for the measured fusion products from the two runs resulted in the present assessment (presented in the following) of the experimental configurations, to try to resolve the discrepancies. This involved detailed consideration of features of the experiments that could have contributed to different final cross sections, which are discussed in Secs. II B3 and II B4. Subsequently, Sec. III uses the empirical systematics from all the ^{9}Be + ^{209}Bi measurements to resolve problems

relating to (i) relative yields of xn channels following complete fusion, (ii) efficiency of observing complete fusion products, (iii) absolute normalization, and (iv) the fission contribution to the complete fusion cross sections. Since these procedures result in changes to published cross sections, it is necessary to describe in detail the arguments and procedures used.

Having applied corrections to the experimental cross sections, we present the new cross sections in Sec. III B, and their interpretation is described in subsequent sections.

1. Complete fusion products

The CF measurements for ^{9}Be + ^{209}Bi show that the complete fusion products ^{215,216}Fr make up the majority of the xn evaporation residues, from the fusion barrier energy to ∼15 MeV above (see Fig. 1). As will be shown in Sec. III, decay from these nuclei should also dominate the α spectra for the ^{10,11}Be reactions in the same energy regime. Charged particle evaporation following complete fusion is also possible; however, measured evaporation yields from reactions where ICF is expected to be negligible provide upper limits to the yields expected in these Be reactions. In Ref. [3], measurements for the ^{13}C + ^{204}Hg reaction forming ^{217}Rn showed that there should be <3% of charged particle evaporation products following complete fusion in the reaction ^{9}Be + ^{208}Pb. It was shown in Ref. [6] that for the reactions ^{10,11}B + ^{209}Bi at near-barrier energies, the total pxn fraction (forming Rn isotopes) should be less than 1%, and the αxn fraction (forming At isotopes) no more than 3%. For the neutron-rich ^{10,11}Be projectiles, forming compound nuclei with a lower charge, these fractions will be even smaller, and they are thus at an insignificant and undetectable level. Thus it is expected that any significant yield of Rn and At seen in the measurements should be associated with ICF, and not CF.

2. Incomplete fusion products

For ^{9}Be + ^{208}Pb, the α-ICF products seen [3] at above-barrier energies were ^{212,211,210}Po. Following the recent work of Ref. [14], these must be associated predominantly with transfer of a neutron followed by capture of a ^{4}He projectile fragment. In the reactions of ^{10,11}Be, the most energetically favorable α-cluster breakup channels are ^{4}He + ^{6}He and ^{5}He + ^{6}He, respectively. By taking into account the Q values and neutron binding energies, the principal evaporation products following α-ICF for ^{10,11}Be + ^{209}Bi are likely to be ^{214,213,212,211}At. Only the heavier isotopes ^{214,213}At were detectable in these experiments (see Fig. 3), and these are likely to be the major component of the heavy α-ICF products only at the lower beam energies. Thus neither experiment R1 nor R2 offers full efficiency for α-ICF, if present.

3. Alpha detection efficiency within time windows

The efficiency for detecting a given decay following formation depends on the lifetime of the decay and the time window for detection. In R1, the time window was 1800 ns wide, whereas in R2, it was 400 ns. By allowing a 20-ns veto of prompt particles, the detection efficiencies associated with these time windows are presented in Fig. 3, for the heavy complete and incomplete fusion products whose efficiency is
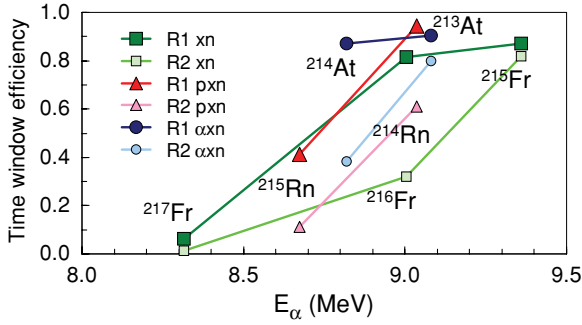
FIG. 3. (Color online) Probability of detecting α particles from the nuclei indicated, within the different data acquisition time windows associated with the two experiments (R1 [17] and R2 [18]) in which ^{10,11}Be fusion was measured. The key difference between the the two runs is the different ^{216}Fr efficiencies (dark and pale green squares).

high enough that detection was in principle possible. These products are expected to make a major contribution to CF and ICF for the ^{10,11}Be + ^{209}Bi reactions, as discussed in detail in the following. For both CF and ICF products, there is a significant difference in the time window efficiencies between R1 and R2, as shown in Fig. 3. This results from the narrower time window in the latter experiment. For the complete fusion-xn channels, the efficiency for ^{216}Fr ($E_\alpha =$ 9.005 MeV) and ^{215}Fr ($E_\alpha =$ 9.360 MeV) are 0.81 and 0.87, respectively, in Run 1, whereas for Run 2 they are 0.32 and 0.82, respectively. Thus in Run 1, assignment of the α yield to either ^{216}Fr or ^{215}Fr is not very important in determining the xn cross sections, but it is vital in Run 2. Unfortunately, there was a much higher risk of incorrect assignment in Run 2, resulting from the geometry of the detectors, as described in the following.

4. System energy response

The use of a catcher foil in general limits the effective energy resolution of the detectors measuring the decay α particles, owing to the energy lost by the α particles traversing the catcher foil. This effect can be large when the α particles are detected at a large range of angles to the normal to the target-catcher sandwich and/or when the target itself is thick.

In Run 1, the targets were angled at 45° to the beam and at 45° to the normal to the 4.8-cm square Si detectors. From the detector geometry and 33% solid angle described in Ref. [17], it is estimated that the detectors counted α particles up to $\sim$55° from the normal to the catcher foil, corresponding to a maximum energy loss of 1.74 times that at the target normal, or a maximum energy spread of 0.74 of the smallest energy loss.

In contrast, in Run 2 the Si detector solid angle was almost doubled [18], and the targets and catcher foils were normal to the beam. We estimate the range of angles to the target normal to be from 27° to 72°. This corresponds to energy losses between 1.12 and 3.17 of that at the normal, or a spread of 2.05 times the minimum energy loss. This helps to explain why the α-particle energy spectra from Run 2 hardly show distinct peaks [18], unlike the spectra from Run 1 [17].
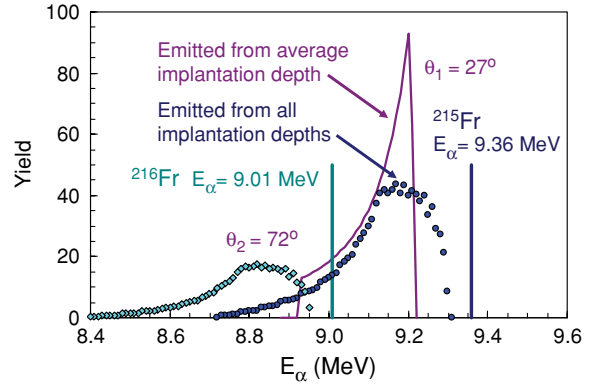

FIG. 4. (Color online) Expected α-particle energy spectra for Run 2, detected over the angular range 27° to 72° to the target normal (see text). For the same primary production of ^{215,216}Fr (vertical blue and turquoise lines, respectively), the narrow time window in R2 leads to only $\sim$40% of the ^{216}Fr α particles (pale turquoise diamond-shaped symbols) being detected compared to ^{215}Fr (dark blue circles).

In the analysis of Run 2, the yields of the major α peaks (the 9.360-MeV line from ^{215}Fr and the 9.005-MeV line from ^{216}Fr) were obtained by fitting overlapping Gaussian peaks to the measured energy spectra. To investigate whether a Gaussian functional form is appropriate, particularly for the detector geometry of Run 2, an analytical form for the energy response was sought, by making the simplifying assumption that the azimuthal angular acceptance is independent of the angle θ with respect to the normal to the catcher, which is a good approximation for Run 2.

The spectrum of counts versus energy loss of the α particles ($d\sigma/dE_{\rm loss}$) can be written as

$$d\sigma/dE_{\rm loss} = (d\sigma/d\theta)(d\theta/dE_{\rm loss}). \quad (1)$$

For α decay, the emission is isotropic, and thus $d\sigma/d\theta \propto \sin\theta$. The energy loss is proportional to $1/\cos\theta$ and thus $dE_{\rm loss}/d\theta \propto d(1/\cos\theta)/d\theta$, giving $d\theta/dE_{\rm loss} \propto \cos\theta/\tan\theta$. Thus $d\sigma/dE_{\rm loss} \propto \cos^2\theta$, which can be rewritten in the desired form $d\sigma/dE_{\rm loss} \propto 1/E_{\rm loss}^2$.

The full curve in Fig. 4 shows the spectrum expected in Run 2 for 9.360-MeV α particles from ^{215}Fr, if one assumes emission only from the average implantation depth, for a 45-MeV ^{10}Be beam energy. The realistic energy spectrum, shown by the dark circles in the figure, was obtained by dividing the Bi target into ten layers and taking the production cross section to be independent of depth in the target and thus $E_{\rm loss}$. This results in a very asymmetric function, with a significant width. Indeed, there is considerable overlap with the spectrum calculated for the 9.005-MeV α particle from ^{216}Fr (pale diamonds). This overlap leads to the expectation that even when the ^{216}Fr yield is actually zero, a Gaussian fit at the energy of the maximum of the expected yield will still return substantial counts. Combined with the much lower time window efficiency of α particles assigned to decay of ^{216}Fr (accounted for in the simulation in Fig. 4), substantial overestimation of the ^{216}Fr cross section can easily occur. Indeed, comparison of the cross sections from Run 1 and Run 2, carried out in the following, shows large discrepancies

that are very likely to originate from the wide asymmetric energy response resulting from the experimental arrangement in Run 2. On this basis, corrections are applied to obtain revised cross sections for Run 2, as described later.

III. SYSTEMATIC ANALYSIS OF EXPERIMENTAL RESULTS

A. ^{10,11}Be measurements

The experimental data from the original analysis of Run 1, published in Ref. [17], is denoted in the figure legends of this work as R1 1996. In that analysis, the α spectra (shown in Fig. 1 of Ref. [17]) were divided into only two components, associated with ^{215}Fr ($E_\alpha = 9.360$ MeV) and ^{216}Fr ($E_\alpha = 9.005$ MeV). The energy resolution was given as 150 keV; thus these yields would also probably include decay α particles following α-ICF observable within the experimental time window. If no such α-ICF were present, complete fusion and total fusion would be the same, and the measured yields would correspond to complete fusion. The experiments were unable to detect the lighter At α-ICF products ^{212,211}At. These are most likely to be produced at the higher beam energies. Thus if α-ICF were present with significant yield, the total measured fusion product cross sections would be larger than those for CF alone. However, at the higher energies they would be smaller than the total fusion cross section. Owing to remaining uncertainty of the true situation, the experimental cross sections from these Run 1 data will be referred to subsequently as total fusion.

The most recent analysis of the same Run 1 data was reported in 2004, in Ref. [18], denoted here as R1 2004. In that analysis, narrower beam energy bins were applied, and the α-spectra were fitted by four Gaussian peaks, the same Fr peaks as previously, and also ^{214}At ($E_\alpha = 9.080$ MeV) and ^{213}At ($E_\alpha = 8.819$ MeV), both associated with α-ICF. The energy resolution here was given as 104 keV. The cross sections assigned to Fr in that analysis exclude any α-ICF, and must be associated with capture of all the charge of the projectile. They will here be referred to as complete fusion, though whether the weakly bound neutron in ^{11}Be is captured cannot be determined from these results alone.

The more recent measurements from Run 2, also reported in Ref. [18], are denoted on figure legends as R2 2004. Because of the poor effective energy resolution (discussed in Sec. II B 4), the α spectra (shown in Fig. 3 of that work) were divided only into the two Fr components and should be equivalent to the R1 1996 cross sections, if one takes into account the lower efficiency for ^{216}Fr (discussed in Sec. II B 3).

1. Components of complete fusion cross sections

The first step in the assessment of the fusion cross section systematics is to investigate the relative yields of the ^{215,216}Fr complete fusion products, which are independent of the issue of the absolute normalization. The latter is discussed after the division of cross section between the xn products is resolved.

The measured xn fractions determined from the cross sections presented in the three analyses described here are
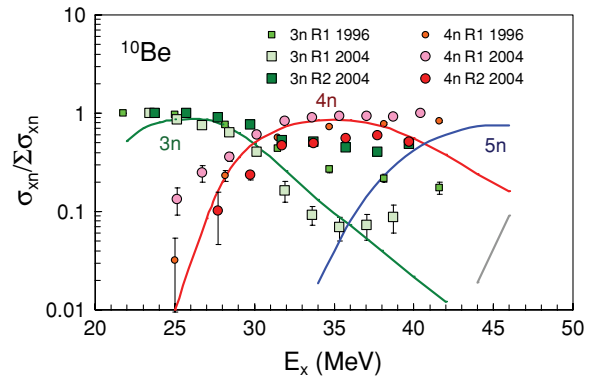

FIG. 5. (Color online) The same as Fig. 1, but for the reaction ^{10}Be + ^{209}Bi. Square points represent the measured fraction of ^{216}Fr; circles correspond to those of ^{215}Fr. The small symbols correspond to the measurements (labeled R1) of Ref. [17], the larger symbols correspond to the reanalysis of those measurements described in Ref. [18], and the large dark symbols represent the measurements (R2) of Ref. [18]. Each shows somewhat different behavior, though there is broad agreement with the expected trends shown by the smooth curves from Fig. 1 (see text).

shown for ^{10}Be + ^{209}Bi in Fig. 5, and for ^{11}Be + ^{209}Bi in Fig. 6, as a function of the compound nucleus excitation energy E_x. Because compound nucleus decay is expected to be independent of the method of formation, and the angular momentum distributions are similar in all three reactions, at the same E_x the decay processes should be similar for all three reactions. By taking into account the fusion Q value and neutron binding energies, it is possible to estimate the expected excitation energy shift in the evaporation fractions from those measured for ^{9}Be + ^{209}Bi. For the $4n$ channel (dominant in all reactions just above the barrier, and detected in all measurements), there is negligible E_x shift between the ^{9}Be and ^{10}Be reactions. In Fig. 5 the curves from Fig. 1 are thus presented with no E_x shift. From Q values, the expected E_x shift between the ^{9}Be and ^{11}Be $4n$ evaporation channels is -4.9 MeV. Since this is quite a large shift, the evaporation temperatures and thus mean neutron kinetic energies should be lower for the ^{11}Be reaction, estimated to be ~0.2 MeV for each neutron. Thus the expected E_x shift becomes close to -4 MeV, which is the value used in Fig. 6.

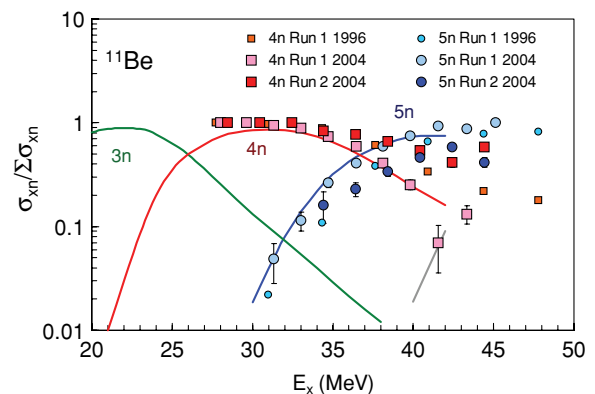FIG. 6. (Color online) The same as Fig. 5, but for the reaction ^{11}Be + ^{209}Bi (see text).

At the lower energies, the experimental data for both reactions agree quite well with these curves; however, at the higher energies, the measurements only agree for the R1 2004 analysis, with apparently excessive yield assigned to ^{216}Fr (corresponding to the $3n$ channel for ^{10}Be and to $4n$ for ^{11}Be), particularly in R2 2004. It was noted in Ref. [18] that for ^{10}Be + ^{209}Bi there is a significant discrepancy at the higher energies between the $3n$ channel cross sections determined from the R1 2004 and R2 2004 analyses, and a possible explanation was given: "[I]n the Gauss fitting procedure there might be, in the area of the ^{216}Fr peak, some contamination from ^{215}Fr." The calculations in Sec. II B4 of this work show quantitatively that this is indeed a very significant issue. The same phenomenon should be present in the $4n$ channel for ^{11}Be + ^{209}Bi, since this also corresponds to the α decay of ^{216}Fr, and the same behavior is indeed visible in Fig. 6. Note that the ratio of the $4n$ to $5n$ cross sections was used in Ref. [17] to infer the behavior in fusion of the halo neutron of ^{11}Be. These ratios are different in the R1 2004 analysis, and thus the conclusion of Ref. [17] must be brought into question by the later analysis [18] of the same data.

It should be possible to make corrections for this experimental effect if the E_x dependence of the ratio of the observed xn cross sections can be predicted. Here the detailed measurements for ^{9}Be + ^{209}Bi can be used to empirically predict the behavior for the other two reactions. In the upper panel of Fig. 7, the ratios of the $3n$ to $4n$ cross sections (the measured channels for ^{10}Be + ^{209}Bi) are shown as a function of E_x. The data for several ^{9}Be + ^{209}Bi measurements are shown by dark circles. Extensive data also exist for ^{9}Be + ^{208}Pb [3,4,16]. By making the same E_x mapping as described before, with the expected E_x shift of -1 MeV, these data (smallest circles) coincide with those for the Bi target. The trend of all these data is represented by the smooth full curve. As previously described, the expected E_x shift between ^{9}Be + ^{209}Bi and ^{10}Be + ^{209}Bi is negligible, and thus the same curve was used to predict the $3n/4n$ ratio for the ^{10}Be reaction. The R1 2004 data (complete fusion only) agree quite well with the prediction, but the R2 2004 data lie up to 10 times higher at the highest E_x.

The lower panel in Fig. 7 shows the $4n/5n$ ratio for ^{11}Be (diamonds and triangles) and ^{9}Be (circles), the dashed line being a smooth representation of the trend for the latter data. The full curve shows the expectation for ^{11}Be, accounting for the E_x shift between ^{9}Be and ^{11}Be of -4 MeV. The R1 2004 data coincide extraordinarily well with this prediction, but the R2 2004 data deviate increasingly from the curve with increasing E_x, as for ^{10}Be. This deviation, for both projectiles, is consistent with quantitative expectations based on the asymmetric energy response inherent in Run 2.

As pointed out in Sec. II B3, the assignment of cross section between ^{215}Fr and ^{216}Fr is not important in determining the fusion cross sections in Run 1, but it is crucial for Run 2. To obtain corrected cross sections for Run 2, the ^{215}Fr and ^{216}Fr cross sections from the R2 2004 analysis were converted to total observed counts by using the calculated time window efficiencies, and the counts were redistributed between the two channels according to the ratios expected from Fig. 7, including the time window efficiency correction. Then the
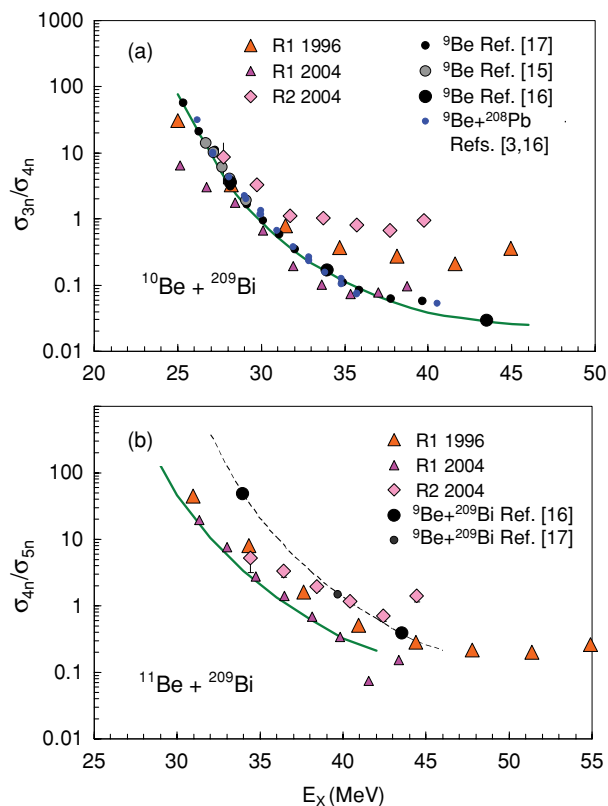

FIG. 7. (Color online) Ratio of the two observed xn cross sections as a function of CN excitation energy E_x for the ^{10}Be (upper panel) and ^{11}Be (lower panel) reactions. Blue circles represent the experimental ratios for ^{9}Be + ^{208}Pb, black and grey circles those for ^{9}Be + ^{208}Pb. The dashed line shows the trend of the ^{9}Be data, and the full curves show the predictions, based on these results, for the radioactive beam reactions, with the different fusion Q values and neutron binding energies taken into account (see text). The experimental values for the latter reactions, from the different experiments and analyses, are indicated by the orange and magenta triangles and pink diamond symbols as indicated.

counts were converted back to individual cross sections for ^{215}Fr and ^{216}Fr. These will be denoted as "R2 Reanalysis" in subsequent figure legends. Naturally their ratios lie precisely on the full curves in Fig. 7. The xn fractions were not changed for the fusion cross sections indicated in the figures by R1 1996 (where the division hardly affects the cross section) or for the original R2 2004 analysis.

2. Evaporation residue total cross sections

A final important correction to obtain the evaporation residue cross sections following complete fusion is to account for the fraction of the total yield of Fr isotopes that the measured ^{215}Fr and ^{216}Fr channels comprise. This is another correction where the detailed and precise measurements available for ^{9}Be + ^{209}Bi are useful. Figure 8 shows experimental values of the ratio of $(3n + 4n)$ cross sections to the total xn cross section, and the $(4n + 5n)$ cross sections to the total, from the various ^{9}Be + ^{209}Bi measurements [15–18]. Although measured as a function of the excitation energy for
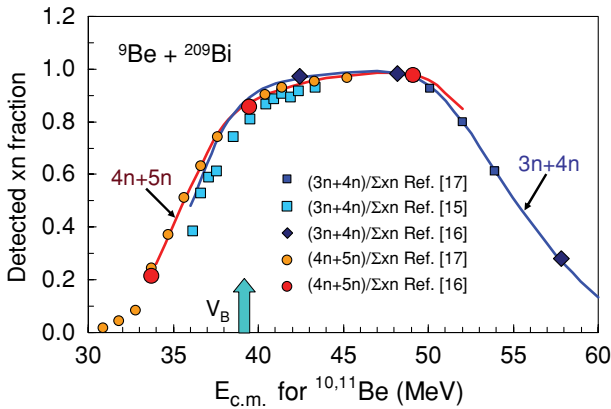
FIG. 8. (Color online) Ratios of the complete fusion cross sections found in the summed 3n and 4n channels (blue and turquoise squares and diamonds), and the 4n and 5n channels (red and orange circles), to the total xn cross sections. The data points are from the indicated measurements for the ^{9}Be + ^{209}Bi reaction. They are plotted against the corresponding c.m. energies for the ^{10}Be and ^{11}Be reactions, respectively (see text). The expected energy region of the fusion barriers are indicated by the wide arrow labeled V$_B$. The curves were used to estimate the efficiencies for detecting complete fusion products for both reactions.

the ^{9}Be + ^{209}Bi reaction, for convenience they are plotted against the center-of-mass energies for the ^{10}Be and ^{11}Be reactions, respectively. These energies were determined by applying the same energy shifts as were applied to the excitation energy scales in Figs. 5, 6, and 7. This then gives a clear view of the $E_{c.m.}$ range for each reaction where the measured ^{215,216}Fr cross sections are a good representation of the total Fr yield. The correction of the measurements to account for the unobserved Fr isotopes is estimated to be sufficiently reliable at energies where the efficiencies drop to 0.7 for ^{10}Be ($3n + 4n$) and 0.8 for ^{11}Be ($4n + 5n$). The full lines, determined from the smooth curves in Fig. 1, were used to determine the total Fr isotope cross sections for the ^{10}Be and ^{11}Be reactions. The presence of a fraction of α-ICF in the previous ^{9}Be + ^{209}Bi 2n cross sections [16] causes a few-percent drop in the apparent experimental efficiency at the lower energies for the ($3n + 4n$) ratio. The efficiencies used account for this fact, and thus the curve lies slightly above the experimental points from the previous experiments. The correction for the fraction of the total xn yield that could be measured was applied to all the fusion cross sections that are presented subsequently.

Finally, to obtain the total evaporation residue cross sections, the overall normalization of the data must be considered. In Ref. [18], it was noted that the ^{11}Be cross sections from Run 1 presented in previous papers were a factor $\sqrt{2}$ too large. This was due to omitting to account for the target in Run 1 being at 45° to the beam [17]. This target angle was also used for the ^{10}Be and ^{9}Be measurements at RIKEN, and thus the cross sections for all RIKEN data from Run 1 should be multiplied by $1/\sqrt{2}$ [19]. It was recently shown in Ref. [16] that the previous RIKEN 3n cross sections for ^{9}Be + ^{209}Bi [17], when corrected by the $1/\sqrt{2}$ factor, are in good agreement with the most recent measurements (with

reliable absolute normalization [16]), supporting the intrinsic accuracy of the Run 1 RIKEN data. The Run 1 cross sections shown in the next section are multiplied by this factor, except those determined from the results presented in Ref. [18], where this correction had already been made. No correction of this type was necessary for Run 2, where the target foil was at 90° to the beam.

3. Systematics of fission probabilities

Having evaluated the total corrected evaporation residue cross sections, we now need to investigate the systematics of the fission cross sections, since the total fusion cross sections at the highest beam energies should have a substantial contribution from fission, as shown in Fig. 5 of Ref. [18]. The Run 1 fission cross sections were presented in that work, and thus they are presumably already scaled by the $1/\sqrt{2}$ factor. These fission cross sections have been divided by the sum of the corrected total evaporation residue and fission cross sections to give the fission probabilities, which are shown in Fig. 9. The Run 1 probabilities for both ^{10}Be and ^{11}Be projectiles are consistently a factor of 2 or more larger than those from Run 2, strongly suggesting that one of the data sets is in error. Systematics can help to determine which data sets are more likely to be correct.

The fission probabilities following complete fusion for the ^{9}Be + ^{209}Bi reaction, measured at the ANU [16] (larger squares in Fig. 9) agree well with the previous measurements of Ref. [17] (small squares); their trend is given by the full curve in the figure. The fission probabilities for the reactions with the more-neutron-rich Be isotopes, forming less fissile compound nuclei, should lie lower. The dashed lines show trend lines for the ^{10,11}Be data from Run 2, which are in good agreement with this expectation, and thus it must be concluded that the fission cross sections from Run 1 are about a factor
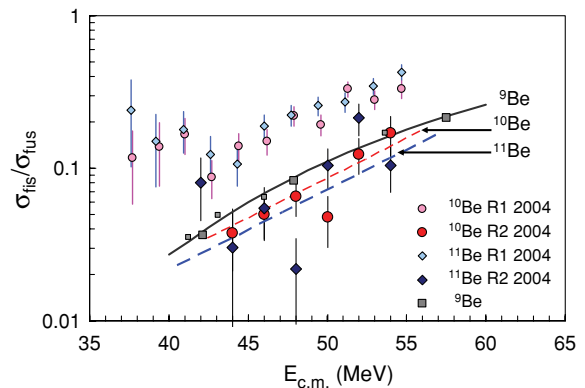

FIG. 9. (Color online) Ratios of measured fission to fusion cross sections. Data are shown for the Run 1 measurements (small circle and diamond symbols) as reported in 2004 (R1 2004) and from Run 2 (large circle and diamond symbols) also reported in 2004 (R2 2004). The gray square data points indicate the experimental fission probabilities for complete fusion for ^{9}Be + ^{209}Bi from Refs. [16,17]; the full curve is drawn to guide the eye. The fission probabilities for ^{10,11}Be + ^{209}Bi (red and blue, respectively) should lie below this line, favoring the Run 2 data. The adopted probabilities in this work are given by the dashed lines (see text).

of 2 too large. This could possibly have come about because the fission events were measured in singles in Run 1 but in coincidence in Run 2.

Although the experimental fission probabilities from Run 2 show the expected trends, they do show considerable scatter. Thus the fission contribution to the fusion cross sections for all the cross sections presented subsequently for both Run 1 and Run 2 were determined in this work by using the exponential functions (dashed lines) that describe the average trends of the Run 2 measurements.

B. Total fusion cross section systematics

Having applied corrections to the absolute cross sections, based on the expectation of systematic behavior from one isotope to the next, we can now compare the data from the different analyses for consistency, before proceeding to interpretation of the results.

1. Experimental results

Figure 10 shows in the upper two panels the absolute cross sections attributed to the complete fusion 3n and 4n channels for the ^{10}Be + ^{209}Bi reaction. Figure 11 similarly shows the 4n and 5n cross sections for the ^{11}Be + ^{209}Bi reaction. For Run 1, the division between 3n and 4n for ^{10}Be (4n and 5n for ^{11}Be) does not materially affect the total evaporation residue yields but, as has been emphasized, is important in Run 2. From the cross section ratios, the original analysis of the Run 2 data (R2 2004) assigned too much yield to the 3n (4n) channel at the higher ^{10}Be (^{11}Be) energies, which is rather obvious in the top panel of the figures. By using the expected 3n/4n (4n/5n) ratios, the approach taken in this work gives significantly lower cross sections for the 3n (4n) channel and somewhat higher ones for the 4n (5n) channel. The total fusion cross sections in the bottom panels are obtained by applying the efficiency factors from Fig. 8 to the summed 3n and 4n cross sections for ^{10}Be (Fig. 10) and the 4n and 5n cross sections for ^{11}Be (Fig. 11), and by adding on the fission cross section determined as described earlier.

Because of the excessive cross section attributed in the 2004 analysis of Run 2 to the 3n (4n) channel, whose detection efficiency in the time window was small, these fusion cross sections (R2 2004, denoted by pink circles) should not be considered reliable. Rather the new analysis of these data (R2 Reanalysis) and the (here modified) original analysis of Run 1 (R1 1996) should be compared; both assign all observed α decays to the fusion cross sections and, as discussed previously, apart from the possible production at the higher beam energies of the isotopes ^{211,212}At through the α-ICF process, thus should represent the total fusion cross section. These cross sections are given in Table I.

2. Comparison with calculations

Fusion cross sections expected in the absence of breakup were calculated using the code CCFULL [20]. Since only above-barrier cross sections were to be compared, no couplings were included. The Woods-Saxon nuclear potential parameters that were used ($V_0 = 208$ MeV, $r_0 = 1.10$ fm, and
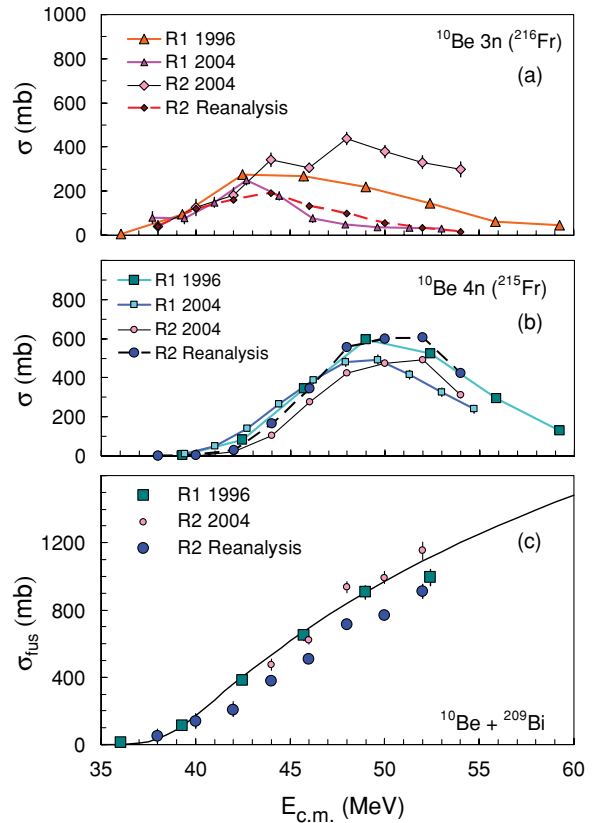

FIG. 10. (Color online) Cross sections for the ^{10}Be + ^{209}Be reaction, showing individual cross sections for (a) ^{216}Fr (3n) and (b) ^{215}Fr (4n), respectively. Data from Run 1 are as analyzed in Ref. [17] (labeled R1 1996) and in Ref. [18] (R1 2004), but components of both are renormalized (see text). Data from Run 2 are as analyzed in Ref. [18] (R2 2004) and in the present work (R2 Reanalysis). (c) The total fusion cross sections from each work, but using fission cross sections from this work in all cases (see text). The full line shows the expectation for fusion in the absence of breakup, using scaled barrier energies (see text).

$a_0 = 0.63$ fm) gave an uncoupled barrier of 38.3 MeV for the ^{9}Be + ^{208}Pb reaction, agreeing with the experimentally determined average barrier [3]. The same potential parameters were used to predict the average barriers for the other reactions, giving energies of 38.76, 38.47, and 38.21 MeV for ^{209}Bi + ^{9,10,11}Be, respectively. These calculations are compared with the experimental total fusion cross sections for ^{10}Be in Fig. 10(c) and for ^{11}Be in Fig. 11(c). For ^{11}Be, the R1 1996 and R2 Reanalysis data agree very well with each other, but they lie below the calculations. For ^{10}Be, the R1 1996 data agree well with the calculations, but the R2 Reanalysis data again lie below. In comparison, the R2 2004 cross sections agree well with the calculations for both reactions.

It may be tempting to dismiss the corrections made to the relative xn yields in generating the R2 Reanalysis cross sections, and accept the R2 2004 total fusion cross sections, since they agree with the calculations. However, accepting these total cross sections only for this reason cannot be justified, when the ^{216}Fr components measured in R2 disagree
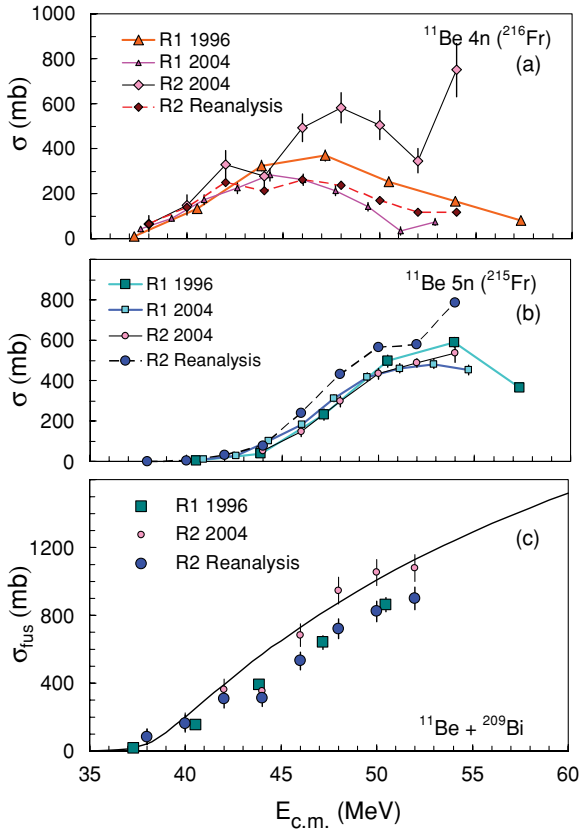
FIG. 11. (Color online) The same as in Fig. 10, but for the ^{11}Be + ^{209}Be reaction, showing the same fusion products, corresponding here to the 4n and 5n channels.

rather badly with the R1 measurements [as seen in panel (a) of the figures], and with expectations from the ^{9}Be measurements.

In any case it must be accepted that the R1 and R2 cross sections are not consistent for one of the reactions. As pointed out previously, the fact that the experimental time window efficiencies for the two measured α peaks was essentially the same makes the results from R1 intrinsically less sensitive to the α energy response resulting from the target-catcher and detector's relative geometry. This fact would favor the results from R1 over those from R2. This is rather unfortunate, as in R2, efforts were made to increase the statistics, but at the cost of a poorer energy response. As in γ-ray spectroscopy, it seems selectivity beats statistics in all but the simplest situations.

C. Systematics of fusion barrier energies

From the preceding discussions, there are two questions that can be asked regarding the total fusion cross sections. The first is whether the channels that could be measured constitute the vast majority of the total fusion products. From the systematic analysis, based on the measured ^{9}Be fusion products, it was concluded that only α-ICF products, if ICF occurs, may be missed, predominantly at the higher energies. The second question, always present for absolute cross-section measurements, if whether the absolute normalization is correct.

TABLE I. Evaporation residue and total fusion cross sections for the ^{10,11}Be + ^{209}Bi reaction as evaluated in this work, as a function of center-of-mass energies $E_{\mathrm{c.m.}}$. The top six data points are from Run 1, using the fission probabilities assigned in this work. The remainder (in 2-MeV energy steps) are from Run 2, using the xn yields and fission probabilities from the reanalysis described in this work. The quoted errors reflect only statistical uncertainties.

	^{10}Be			^{11}Be	
$E_{\mathrm{c.m.}}$ (MeV)	σ_{ER} (mb)	σ_{Fus} (mb)	$E_{\mathrm{c.m.}}$ (MeV)	σ_{ER} (mb)	σ_{Fus} (mb)
36.04	12 ± 9	12 ± 9	37.27	15 ± 8	15 ± 8
39.30	110 ± 10	113 ± 11	40.52	149 ± 14	152 ± 14
42.46	368 ± 25	381 ± 25	43.88	376 ± 31	390 ± 32
45.72	616 ± 31	650 ± 33	47.18	608 ± 38	641 ± 40
48.98	836 ± 37	905 ± 40	50.49	789 ± 39	854 ± 41
52.40	879 ± 43	994 ± 48			
38.00	51 ± 37	52 ± 38	38.00	83 ± 44	84 ± 45
40.00	134 ± 39	138 ± 40	40.00	160 ± 49	164 ± 50
42.00	198 ± 34	205 ± 35	42.00	300 ± 53	309 ± 54
44.00	363 ± 26	379 ± 27	44.00	301 ± 48	312 ± 49
46.00	481 ± 19	510 ± 20	46.00	509 ± 50	532 ± 52
48.00	663 ± 24	716 ± 25	48.00	681 ± 56	721 ± 59
50.00	698 ± 26	767 ± 28	50.00	765 ± 56	825 ± 60
52.00	800 ± 37	913 ± 42	52.00	818 ± 57	900 ± 63

First, a comparison of the fusion barrier energies for ^{10}Be + ^{209}Be and ^{11}Be + ^{209}Be is made independent of the absolute normalization. If the barrier energies were the same, the total fusion cross sections should be essentially the same. The ratios of the cross sections for ^{11}Be to ^{10}Be were evaluated as a function of energy, separately for R1 and R2. Where the beam energies did not match, linear interpolation was used. The results are shown in Fig. 12. The R1 data show the ratio decreasing toward lower $E_{\mathrm{c.m.}}$, suggesting that the barrier
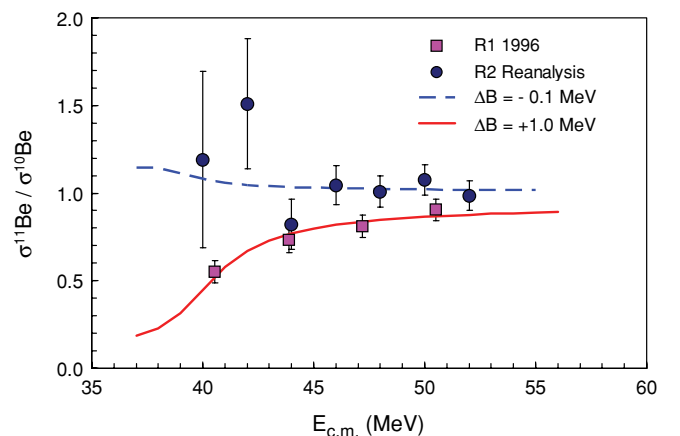

FIG. 12. (Color online) Ratio of ^{11}Be to ^{10}Be total fusion cross sections as a function of energy, from data of Run 1 (magenta squares) and Run 2 (blue circles). The dashed line shows the cross-section ratios calculated for a fusion barrier energy for ^{11}Be, which is 0.1 MeV lower than for ^{10}Be, matching well the Run 2 data. The full line corresponds to a barrier energy for ^{11}Be, which is 1.0 MeV higher, which reproduces the Run 1 data (see text).
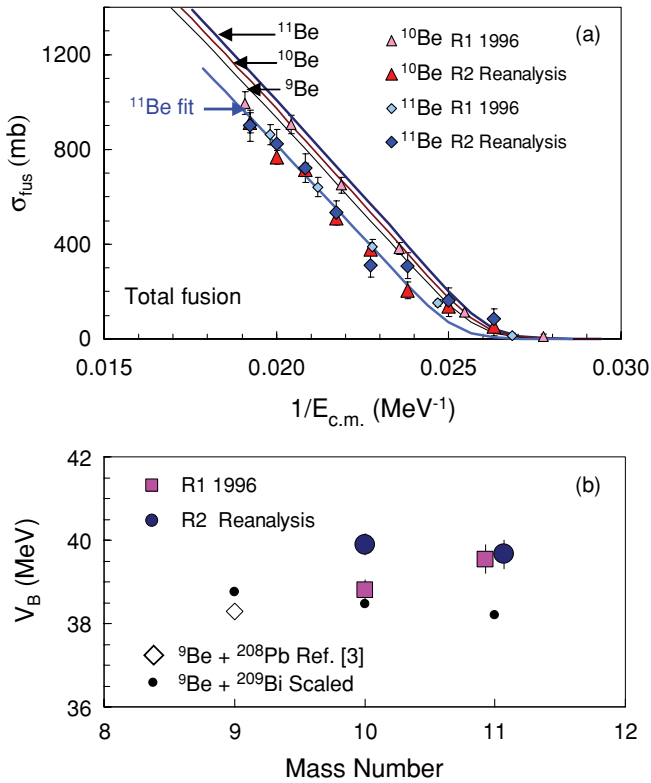
FIG. 13. (Color online) (a) The most reliable total fusion cross sections for ^{10}Be + ^{209}Be from R1 and R2 (pink and red triangles, respectively), and ^{11}Be + ^{209}Be (blue diamonds), as a function of the inverse of the beam energy. The CCFULL fusion excitation functions for ^{9,10,11}Be are shown by the upper three lines. The lower (blue) line labeled "^{11}Be fit" is that reproducing the ^{11}Be R2 data, having a higher barrier energy (see text). (b) The experimental fusion barrier energy for ^{9}Be + ^{208}Pb from Ref. [3] (open diamond) and scaled barrier energies (small black circles) for ^{9,10,11}Be + ^{209}Bi (see text). The experimental barrier energies extracted in this work for ^{10,11}Be from Runs 1 and 2 are shown by the large points.

energy for ^{11}Be is higher than for ^{10}Be. However, the R2 data show a ratio consistent with unity, within uncertainties. Using a reference fusion barrier energy of 38.8 MeV for ^{10}Be + ^{209}Bi (see the following) we calculated the ratios of total fusion cross sections using the code CCFULL. The fit to the R2 data (blue dashed line) showed the barrier energy for ^{11}Be to be 0.10 ± 0.35 MeV *lower* than for ^{10}Be. However, for the R1 data, the barrier energy for ^{11}Be is found to be 0.98 ± 0.24 MeV *higher* than for ^{10}Be. The uncertainties were conservatively assigned corresponding to a χ^2 per degree of freedom of unity, from minima of 0.35 (R1) and 0.7 (R2). This difference in extracted barrier energy must be a reflection of the experimental uncertainties in relative cross sections from the measurements, and it is difficult to understand if the same target was used for both projectiles. Although the two numbers are not consistent within uncertainty, taking a weighted average gives a barrier for ^{11}Be that is 0.63 ± 0.20 MeV *higher* than for ^{10}Be. Considering the conservative assignment of uncertainties, and the previous arguments made for the greater reliability of the R1 data, one can argue that this quoted energy difference should be considered a lower

limit. Thus a comparison of the two reactions independent of absolute normalization suggests a significantly higher barrier for ^{11}Be than for ^{10}Be. This is opposite to expectations if the barrier energy were predicted by scaling by the nuclear radii assuming standard matter density distributions (i.e., according to the projectile and target mass numbers $A_P^{1/3} + A_T^{1/3}$), which would lead to a barrier lower by 0.3 MeV.

Assuming now that the absolute normalization is correct, we fitted the total fusion excitation functions for ^{10,11}Be from the two runs to obtain the individual barrier energies. Figure 13(a) shows the experimental cross sections as a function of $1/E_{c.m.}$. Also shown are the CCFULL calculations of the fusion excitation functions, initially using the scaled barrier energies given in Sec. III B2. A nuclear potential diffuseness of 0.63 fm was employed. The calculations do not match the experimental data. The experimental mean fusion barrier energies were determined by adjusting the radius parameter of the nuclear potential so that the calculation reproduced the excitation function for each reaction. Only measured fusion cross sections above 200 mb were included, to reduce sensitivity to channel couplings [21]. The data from R1 and R2 were treated separately. The best-fitting calculation reproducing the ^{11}Be R1 data is shown by the lowest (blue) curve, labeled "^{11}Be fit". The deduced barrier energies for ^{10}Be were 38.8 ± 0.3 MeV from R1, and 39.9 ± 0.3 MeV from R2, whereas for ^{11}Be they were 39.5 ± 0.4 MeV from R1 and 39.7 ± 0.4 MeV from R2; they are plotted in Fig. 13(b), as a function of the mass number of the projectile. The relative behavior agrees with the conclusions from the normalization-independent analysis performed previously, but here the absolute barrier energies can be compared with those for the stable ^{9}Be projectile. Taking all data to have equal reliability, one can conclude that the barrier energies are similar for all three Be isotopes. However, it can also be said that there is no evidence for a reduction in the mean barrier energy resulting from the neutron halo of ^{11}Be. The deduced barrier energies for ^{10}Be from Run 1 and Run 2 differ by about 1.1 MeV, indicating either that the extracted average barriers for ^{11}Be and ^{10}Be should be assigned such an uncertainty or that one of the barrier energies is in error. From the disagreement of the Run 2 ^{10}Be barrier energy with expectations, and the arguments already made regarding the poorer accuracy expected from Run 2, it is concluded that the barrier energies from Run 1 should be considered more reliable. From the fits to the Run 1 data, the barrier energy for ^{11}Be is found to be 0.7 ± 0.5 MeV higher than that for ^{10}Be. This is consistent with the normalization-independent determination of the difference in barrier energies described earlier.

This new analysis suggests that the fusion barrier energy is increased for the neutron halo nucleus ^{11}Be, as predicted by time-dependent quantal calculations [22,23]. Further measurements would be required to determine reliably whether the predicted barrier increase, of 0.9 MeV for the zero angular momentum barrier (Fig. 5 of Ref. [23]), is quantitatively correct.

D. Complete and incomplete fusion

The 2004 analysis of Run 1 (R1 2004) fitted the measured energy spectra with not only Fr α lines but also At lines [18]. Thus the total Fr yields plus fission (assigned to CF [6])
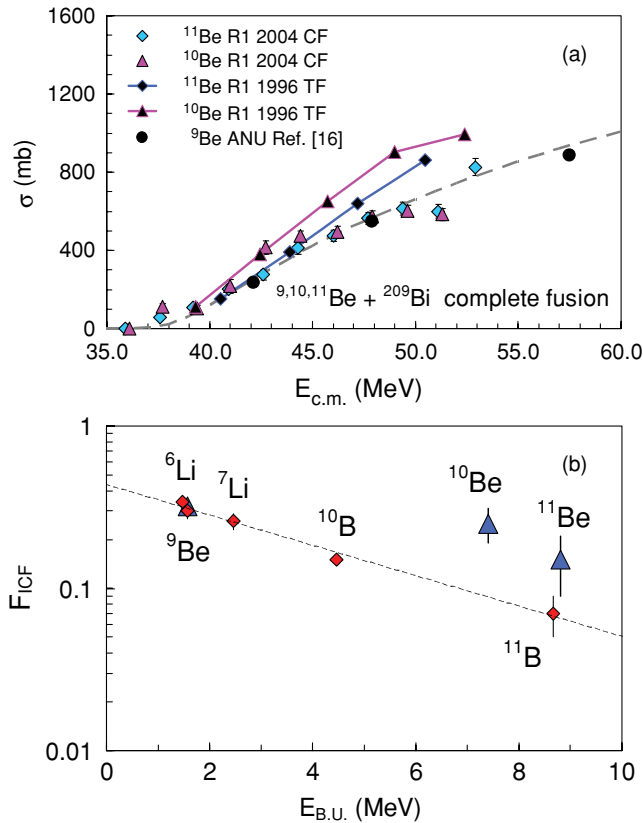
FIG. 14. (Color online) (a) The black-outlined points show the complete fusion cross sections (excluding ICF) for the ^{10,11}Be-induced reactions, determined based on the 2004 analysis of Run 1 data in Ref. [18]. Complete fusion for ^{9}Be + ^{209}Bi is shown by the black circles, with the dashed line showing the estimated energy dependence. The three data sets show unexpectedly good agreement. The ratio to the total fusion cross sections from Run 1 for ^{10,11}Be, shown by the joined dark points, allows estimation of the fraction of ICF, shown in (b) by blue triangles, as a function of the threshold energy for breakup into two charged fragments. The other recent data point, for ^{9}Be (blue triangle), is from Ref. [16]. The diamond-shaped points are from Ref. [6], corresponding to data available at that time for reactions of various projectiles with ^{208}Pb or ^{209}Bi.

should represent complete fusion only, with α-ICF excluded. Indeed, the cross sections are significantly lower—though surprisingly this reduction occurs predominantly at the highest energies, where the detectable At decays should not represent the dominant At isotopes produced. This raises some doubts about the reliability of the fitting process with multiple lines, particularly in view of the asymmetry expected in the energy response of a catcher plus detector system with a wide angular acceptance. Nevertheless, it is of interest to compare these CF cross sections with those for ^{9}Be + ^{209}Bi.

These cross sections are shown in Fig. 14(a) for ^{10,11}Be + ^{209}Bi, together with the ^{9}Be + ^{209}Bi complete fusion cross sections [16]. The former both agree extremely well with the ^{9}Be data, which would suggest that the fraction of ICF was very similar, if the total fusion cross sections for ^{10,11}Be were similar to those for ^{9}Be. The Run 1 total fusion cross sections [shown also in Fig. 14(a)] are smaller for ^{11}Be than for ^{10}Be, and

thus the fraction of α-ICF is actually smaller. These deduced ICF fractions are shown in Fig. 14(b), as a function of the energy threshold for breakup into two charged fragments. Also shown are the systematics from Ref. [6] for reactions of various light nuclei with ^{209}Bi and ^{208}Pb targets, indicating that the fraction of ICF for stable beams shows a strong correlation with the breakup threshold for charged fragment production. Given the breakup thresholds of 7.41 and 8.81 MeV for ^{10,11}Be, respectively, ICF fractions of $\sim$10% might have been expected for ^{10,11}Be, but the values from the analysis of Ref. [18] lie well above these systematics.

Two extreme and opposing explanations for this discrepancy should be discussed. The first is that the asymmetric detector α-energy response function intrinsic to the experiment has led to excessive yield being assigned to the ^{213,214}At ICF products in the Gaussian fitting procedure, and the ICF fraction shown in Fig. 14(b) simply represents an upper limit. The second is that the systematic behavior might not be followed for all nuclei or reactions. This explanation is supported by the recent demonstration [14] that $\sim$90% of all prompt breakup (and thus of ICF) in ^{9}Be reactions follows neutron stripping from ^{9}Be. Thus it is actually the prompt breakup of unbound excited states (resonances) of ^{8}Be that is the dominant mechanism causing the observed $\sim$30% ICF for the ^{9}Be projectile. It is not impossible that the same mechanism could play an important role at least for ^{10}Be, with neutron stripping to excited states in ^{9}Be leading to breakup and ICF. The existing data indicate the intriguing possibility that α-ICF could be much larger than empirical systematics would suggest, but the experimental uncertainties indicate the need for further measurements with a detector system that allows clearer separation of each α line.

IV. SUMMARY

By using the expectation that compound nucleus decay should change systematically from one nucleus to its neighbor, precise measurements of reaction products for the ^{9}Be + ^{209}Bi reaction have been used to guide expectations for reaction products from measurements using low intensity beams of ^{10,11}Be bombarding ^{209}Bi. Revising relative xn yields and fission probabilities based on expectations, and using an updated absolute normalization [18,19], recently independently validated [16], we have determined revised fusion cross sections for the two separate measurements [17,18] of heavy reaction products in the ^{10,11}Be + ^{209}Bi reactions.

Because of the geometrical configurations and measurement time windows of the experiments, it is here concluded that the results from the first measurement [17], with revised normalization [16,18], are the more accurate. The conclusions of Ref. [17] regarding the behavior of the halo neutron in fusion must however be thrown into doubt, since this information was extracted from the measured ratio of xn cross sections, which are very different in the second analysis [18] of the same data.

The threshold energies for the most energetically favorable charged fragment breakup are 1.57, 7.41, and 8.81 MeV, respectively, for ^{9,10,11}Be, in each case for $Z = 2$ fragmentation. Existing systematics would suggest [6] that the latter two

should thus experience only a small fraction of incomplete fusion where an α particle is not captured (α-ICF). With this assumption, and by assuming that the halo neutron of ^{11}Be is captured with the rest of the projectile, revised total fusion cross sections for the two ^{10,11}Be experiments have been determined, using a new systematic analysis based on high-precision ^{9}Be + ^{209}Bi data [16]. From the first experiment [17], believed to have higher accuracy, the revised total fusion cross sections indicate that the fusion barrier energy for ^{10}Be + ^{209}Bi is similar to that expected by scaling from ^{9}Be reactions. In contrast, the barrier for ^{11}Be + ^{209}Bi appears to be $\sim$1 MeV higher than scaling would predict, suggesting that the halo neutron does not reduce the average fusion barrier in this reaction. This behavior is predicted quantitatively in a time-dependent three-body quantal model of fusion of halo nuclei [23].

In the second analysis [18] of the experiment of Ref. [17], the α energy spectrum was fitted with peaks corresponding to decay of short-lived At isotopes as well as the Fr isotopes that can only be produced in complete fusion. The probability of αxn evaporation following complete fusion for such reactions is low [6], and thus the assignment of these At products to α-ICF, is reasonable. Because the α energies from CF and ICF are rather close, the results rely on the energy calibration and peak shapes used being correct. It is not clear how this was assured [18]. By assuming the results to be correct, the yield from the Fr isotopes was summed with the renormalized fission cross sections, and the resulting CF cross sections were obtained, which were substantially smaller than the total fusion determined from the first analysis. From the ratio of CF to total fusion, the ICF fraction could be estimated. Surprisingly this showed $\sim$25% ICF for the ^{10}Be reaction and $\sim$15% ICF for ^{11}Be, compared with 32% for ^{9}Be [16], despite

the much larger charged breakup threshold energies for the unstable Be isotopes. If ICF were so significant, a contribution could be expected from longer lived At isotopes whose decay could not have been detected in the measurement. Thus these ICF fractions would represent a lower limit, as would the total fusion cross sections. Thus the conclusions from the measurements are significantly dependent on the reliability of the separate identification of Fr and At decays.

It is concluded that it would be beneficial to repeat the measurements, in view of the interesting questions regarding the contrasting influence of neutron halo and α-cluster structures on fusion of ^{9,10,11}Be nuclei. The same experimental conditions as used in Run 1, together with a complete simulation of the decay α-particle detector energy response function, would give a significant improvement in accuracy. Further improvements could be made. To obtain better effective α-particle energy resolution, position-sensitive Si detectors would allow correction for the angle of exit of the α particle from the target. A pure beam of ^{11}Be would be beneficial, eliminating the need for a tagged beam, and thus for a narrow ($\sim$microseconds) time window for α-particle detection. This would allow most reaction products to be detected, and clear identification of CF and ICF products could be achieved with improved certainty. Thus experiments could now be performed allowing more reliable conclusions regarding the fraction of ICF present and the energies of the fusion barriers.

[1] J. F. Liang and C. Signorini, Int. J. Mod. Phys. E **14**, 1121 (2005).

[2] W. von Oertzen, M. Freer, and Y. Kanada En'yo, Phys. Rep. **432**, 43 (2006).

[3] M. Dasgupta *et al.*, Phys. Rev. C **70**, 024606 (2004).

[4] M. Dasgupta *et al.*, Phys. Rev. Lett. **82**, 1395 (1999).

[5] V. Tripathi, A. Navin, K. Mahata, K. Ramachandran, A. Chatterjee, and S. Kailas, Phys. Rev. Lett. **88**, 172701 (2002).

[6] L. R. Gasques, D. J. Hinde, M. Dasgupta, A. Mukherjee, and R. G. Thomas, Phys. Rev. C **79**, 034605 (2009).

[7] C. Signorini *et al.*, Eur. Phys. J. A **5**, 7 (1999).

[8] P. R. S. Gomes *et al.*, Phys. Rev. C **73**, 064606 (2006).

[9] A. Mukherjee *et al.*, Phys. Lett. B **636**, 91 (2006).

[10] Y. W. Wu, Z. H. Liu, C. J. Lin, H. Q. Zhang, M. Ruan, F. Yang, Z. C. Li, M. Trotta, and K. Hagino, Phys. Rev. C **68**, 044605 (2003).

[11] D. J. Hinde, M. Dasgupta, B. R. Fulton, C. R. Morton, R. J. Wooliscroft, A. C. Berriman, and K. Hagino, Phys. Rev. Lett. **89**, 272701 (2002).

[12] M. Dasgupta *et al.*, Phys. Rev. C **66**, 041602(R) (2002).

[13] A. Diaz-Torres, D. J. Hinde, J. A. Tostevin, M. Dasgupta, and L. R. Gasques, Phys. Rev. Lett. **98**, 152701 (2007).

[14] R. Rafiei, R. du Rietz, D. H. Luong, D.J. Hinde, M. Dasgupta, M. Evers, and A. Diaz-Torres, Phys. Rev. C **81**, 024601 (2010).

[15] C. Signorini *et al.*, Eur. Phys. J. A **2**, 227 (1998).

[16] M. Dasgupta, D. J. Hinde, S. L. Sheehy, and B. Bouriquet, Phys. Rev. C **81**, 024608 (2010).

[17] A. Yoshida *et al.*, Phys. Lett. B **389**, 457 (1996).

[18] C. Signorini *et al.*, Nucl. Phys. A **735**, 329 (2004).

[19] A. Yoshida (private communication).

[20] K. Hagino, N. Rowley, and A. T. Kruppa, Comput. Phys. Commun. **123**, 143 (1999).

[21] J. R. Leigh *et al.*, Phys. Rev. C **52**, 3151 (1995).

[22] K. Yabana *et al.*, Prog. Theor. Phys. **97**, 437 (1997); Nucl. Phys. A **738**, 303 (2004).

[23] M. Ito, K. Yabana, T. Nakatsukasa, and M. Ueda, Phys. Lett. B **637**, 53 (2006).